

# Bacterial Networks on Hydrophobic Micropillars

Zeinab Jahed,<sup>†</sup> Hamed Shahsavan,<sup>§</sup> Mohit S. Verma,<sup>§</sup> Jacob L. Rogowski,<sup>§</sup> Brandon B. Seo,<sup>§</sup> Boxin Zhao,<sup>§</sup> Ting Y. Tsui,<sup>§</sup> Frank X. Gu,<sup>§</sup> and Mohammad R. K. Mofrad<sup>\*,†,‡</sup>

<sup>†</sup>Molecular Cell Biomechanics Laboratory, Departments of Bioengineering and Mechanical Engineering, University of California Berkeley, 208A Stanley Hall, Berkeley, California 94720-1762, United States

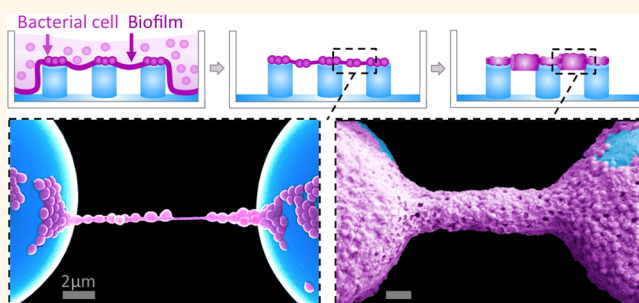
<sup>‡</sup>Molecular Biophysics and Integrated Bioimaging Division, Lawrence Berkeley National Laboratory, Berkeley, California 94720, United States

<sup>§</sup>Department of Chemical Engineering, University of Waterloo, 200 University Avenue West, Waterloo, Ontario N2L 3G1, Canada

## S Supporting Information

**ABSTRACT:** Bacteria have evolved as intelligent microorganisms that can colonize and form highly structured and cooperative multicellular communities with sophisticated singular and collective behaviors. The initial stages of colony formation and intercellular communication are particularly important to understand and depend highly on the spatial organization of cells. Controlling the distribution and growth of bacterial cells at the nanoscale is, therefore, of great interest in understanding the mechanisms of cell–cell communication at the initial stages of colony formation. *Staphylococcus aureus*, a ubiquitous human pathogen, is of specific clinical importance due to the rise of antibiotic resistant strains of this species, which can cause life-threatening infections. Although several methods have attempted to pattern bacterial cells onto solid surfaces at single cell resolution, no study has truly controlled the 3D architectures of growing colonies. Herein, we present a simple, low-cost method to pattern *S. aureus* bacterial colonies and control the architecture of their growth. Using the wetting properties of micropatterned poly(dimethyl siloxane) platforms, with help from the physiological activities of the *S. aureus* cells, we fabricated connected networks of bacterial microcolonies of various sizes. Unlike conventional heterogeneous growth of biofilms on surfaces, the patterned *S. aureus* microcolonies in this work grow radially from nanostrings of a few bacterial cells, to form micrometer-thick rods when provided with a nutrient rich environment. This simple, efficient, and low-cost method can be used as a platform for studies of cell–cell communication phenomena, such as quorum sensing, horizontal gene transfer, and metabolic cross-feeding especially during initial stages of colony formation.

**KEYWORDS:** Bacterial communication, cell patterning, biofilm, microbiome, *Staphylococcus aureus*, antibiotic resistance, methicillin-resistant *Staphylococcus aureus* (MRSA)



The ability of bacterial cells to form microcolonies and biofilms depends on a variety of factors in the cell environment including but not limited to their initial densities and spatial distributions<sup>1–8</sup> and the material and topography of the surface to which they are attached.<sup>9–12</sup> Probing colony dynamics in a controlled manner is of great importance and requires the design of *in vitro* model systems of reduced but relevant complexity to study highly complicated phenomena involved in colony formation. Examples of such phenomena include the formation of short-range direct cell–cell connections for metabolic cross-feeding, protein exchange or horizontal gene transfer,<sup>7,13–17</sup> or long-range communications between spatially separated microcolonies through quorum sensing.<sup>3,18</sup> In addition, these complex communication methods between bacterial cells have allowed them to rapidly

acquire resistance to antibiotics and thus pose a major threat to public health. The emergence of antibiotic resistant bacteria further amplifies the need for developing technologies that can aid us in understanding colony dynamics in these types of bacteria. Specifically, methicillin-resistant *Staphylococcus aureus* remains one of the most dangerous and prevalent causes of infection, which can occur both in health care settings such as medical devices or joint implants, and in the wider community causing complications such as food born illnesses.<sup>19–22</sup> *S. aureus* is a Gram-positive, non-motile, spherical (coccus) bacterium with a diameter of ~500 nm, which forms grape-like clusters on

Received: October 17, 2016

Accepted: January 3, 2017

Published: January 3, 2017

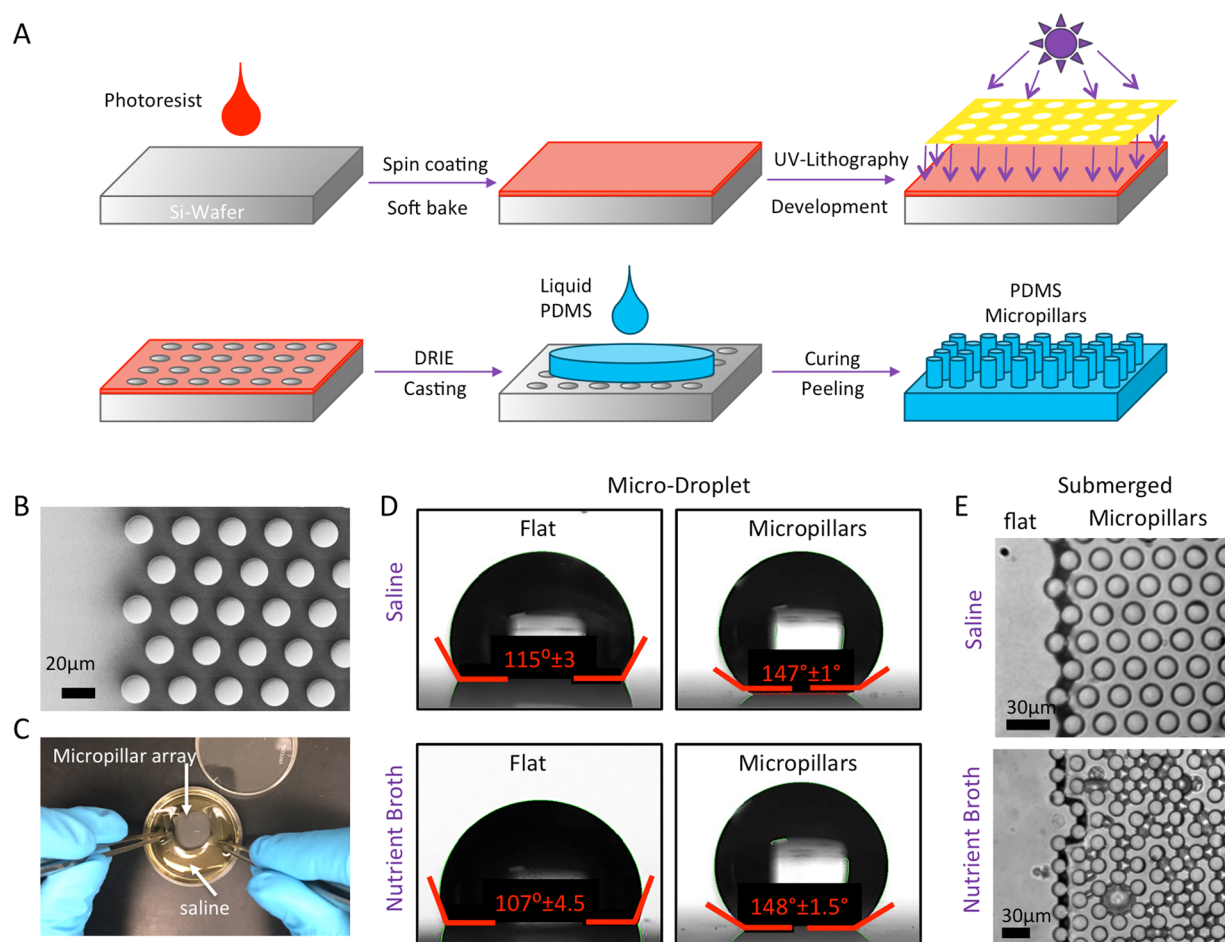


**Figure 1.** PDMS micropillar platform: fabrication and characterization. (A) Schematic representation of the fabrication process of PDMS micropillar arrays. (B) Top view SEM image of the interface between flat PDMS surface and fabricated hexagonally arranged PDMS micropillars arrays. (C) Digital camera image showing the hydrophobic nature of the PDMS platform as solution is repelled from the areas containing micropillars while the platform is pressed down into saline solution. (D) Side view of the dispensed saline and nutrient broth solution droplets for measurements of contact angle on flat and micropatterned PDMS surfaces. (E) Optical image of PDMS micropillars submerged in saline solution (top) and nutrient broth solution (bottom) after 1 h of incubation; the solution is pinned at the interface between the micropillars and the flat PDMS surface in saline, which indicates the presence of air-gaps formed between the micropillars (top). Alternatively after 1 h, the nutrient broth solution begins to penetrate between micropillars (bottom).

solid surfaces. Furthermore, *S. aureus* is a facultative anaerobe meaning that it can grow with or without oxygen.

Several methods have been employed to immobilize and pattern bacteria onto surfaces including dip-pen nanolithography,<sup>23</sup> microcontact printing,<sup>24–26</sup> laser trapping,<sup>1</sup> antibody functionalization of abiotic surfaces,<sup>27</sup> periodic nanostructure arrays,<sup>12</sup> and photolithographic approaches.<sup>28</sup> Although such studies have successfully controlled the spatial organization of surface attached bacterial cells at initial stages of biofilm formation,<sup>9,12,25,27–29</sup> even with single cell resolution, to the best of our knowledge no study has truly controlled the three-dimensional architecture of growing microcolonies or biofilms. Also, most of these methods require rigorous and expensive multiple step processes to pattern bacterial colonies. Moreover, these methods only allow the control of microcolony formation at the solid–liquid interface. However, microcolonies and biofilms can grow at other phase interfaces including liquid–air interfaces (also known as pellicles).<sup>30–32</sup> The mechanisms of the formation of these microcolonies are particularly understudied. In this study, we propose a simple and low-cost physicochemical method, pertaining to both physiology and chemistry, for patterning *S. aureus* cells and controlling the architecture of

microcolonies of *S. aureus* cells on poly(dimethyl siloxane) (PDMS) hydrophobic micropillars. Due to their exceptional wetting properties, micropatterned hydrophobic surfaces have been used for a variety of applications including macroscopic fabrication of one-dimensional nanostructures such as aligned DNA or micellar nanowire arrays.<sup>33–38</sup> Our method takes advantage of the wetting properties of PDMS micropillars as well as the adhesion and biofilm formation of *S. aureus* cells on surfaces to produce nanostrings and rods of *S. aureus* cells.

## RESULTS AND DISCUSSION

**Wetting Properties of PDMS Micropillars by Bacteria Culture Media.** Hexagonally arranged arrays of PDMS micropillars were fabricated using a soft-lithography technique as shown in Figure 1A. The fabricated structures were inspected using scanning electron microscopy (SEM) (Figure 1B). The liquid repellent properties of these platforms were evident from the displacement of saline solution from areas in the center of the platforms that contained micropillars when the platform was immersed into the solution (Figure 1C). To gauge the wettability of the PDMS platform by saline and nutrient broth solutions, which are commonly used for *S. aureus* culture or

**Table 1. Summary of Measured Contact Angle Values for Saline and Nutrient Broth Solutions on PDMS Platforms with Surface Coverage Percentages Ranging from 19% to 33%, and Calculated Theoretical Values for  $r$ ,  $f$ ,  $\theta$ , and  $\theta^{*a}$**

surface coverage (%)	geometrical parameters			nutrient broth			saline		
	$r$	$f$	$\theta^*$ (deg)	$\theta$ (deg)	$\theta^C$ (deg)	$\theta^W$ (deg)	$\theta$ (deg)	$\theta^C$ (deg)	$\theta^W$ (deg)
33	2.96	0.33	105	$107 \pm 4$	140	150	$115 \pm 3$	144	
27	2.62	0.27	108	$107 \pm 4$	144	140	$115 \pm 3$	148	
23	2.36	0.23	111	$107 \pm 4$	147	133	$115 \pm 3$	150	174
19	2.16	0.19	114	$107 \pm 4$	150	129	$115 \pm 3$	153	156

<sup>a</sup> $\theta$  is the Young's contact angle on a flat surface,  $\theta^C$  and  $\theta^W$  are the Cassie–Baxter and Wenzel contact angles, respectively,  $r$  is the roughness factor, and  $f$  represents the area fraction of the liquid–solid interface.

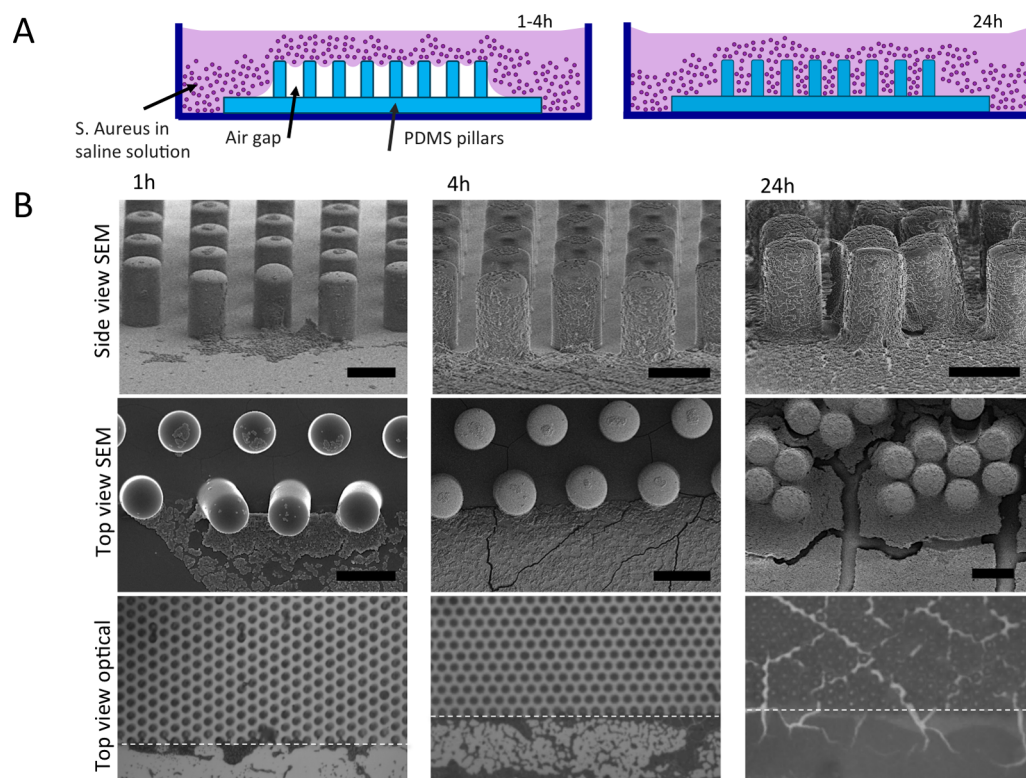


**Figure 2. Formation of *S. aureus* colonies on hydrophobic PDMS micropillars. (A) Schematic representation of the interfaces between the micropillar platform and the solution containing *S. aureus* bacterial cells. The air pockets trapped between PDMS micropillars inhibit the *S. aureus* solution from penetrating between the micropillars. After 24 h, the solution penetrates between micropillars resulting in cell attachment to the micropillar sidewalls as well as the smooth surface between micropillars. Scale bars shown on SEM images represent  $20 \mu\text{m}$ . (B) Representative scanning electron micrograph and optical images of *S. aureus* cells at the interface between PDMS micropillars and their adjacent smooth surfaces. The top row shows a side view SEM image of PDMS micropillars after 1, 4, and 24 h bacteria incubation times at a  $70^\circ$  SEM stage tilt. The second row represents top view SEM images of PDMS micropillar arrays. These images indicate that bacterial cells adhere preferentially to the smooth surface as well as pillar tops after 1–4 h incubation times but penetrate between micropillars and cover the platforms fully after 24 h. Low magnification top view optical microscope images on the third row also show the absence of bacterial cells between micropillars after 1–4 h incubation times but a full coverage of the platform after 24 h of incubation. The white dotted lines indicate the interface between micropillar arrays and the adjacent smooth surfaces. Cracking of the bacteria film and clustering of micropillars seen for 24 h incubation times are likely caused while drying the samples for imaging.**

storage, the shape and contact angles of droplets of saline and nutrient broth were measured on a control flat PDMS as well as micropatterned PDMS samples as shown in Figure 1D. The contact angle of broth on the flat PDMS sample ( $107^\circ \pm 4^\circ$ ) was considerably lower than that of saline ( $115^\circ \pm 3^\circ$ ) (Figure 1D), indicating more repellence between the saline solution and the flat PDMS surface. Micropatterning of the PDMS led to an increase in the contact angles of both liquid probes. The contact angle of the nutrient broth on the micropillar arrays with the highest and lowest surface coverage is  $148^\circ \pm 1.5^\circ$  and  $150^\circ \pm 1.5^\circ$ , respectively. The contact angle of the saline on the

micropillar arrays with the highest and lowest surface density is  $147^\circ \pm 1^\circ$  and  $150^\circ \pm 1^\circ$ , respectively. The increment of contact angles on rough surfaces is a well-known effect, which can be explained by two distinct hypotheses. On the one hand, increase of the roughness can result in the increment of the solid–liquid contact area and consequently hydrophobicity.<sup>39</sup> This is known and formulated as the Wenzel regime of liquid–solid contact as shown below:

$$\cos \theta^W = r \cos \theta$$

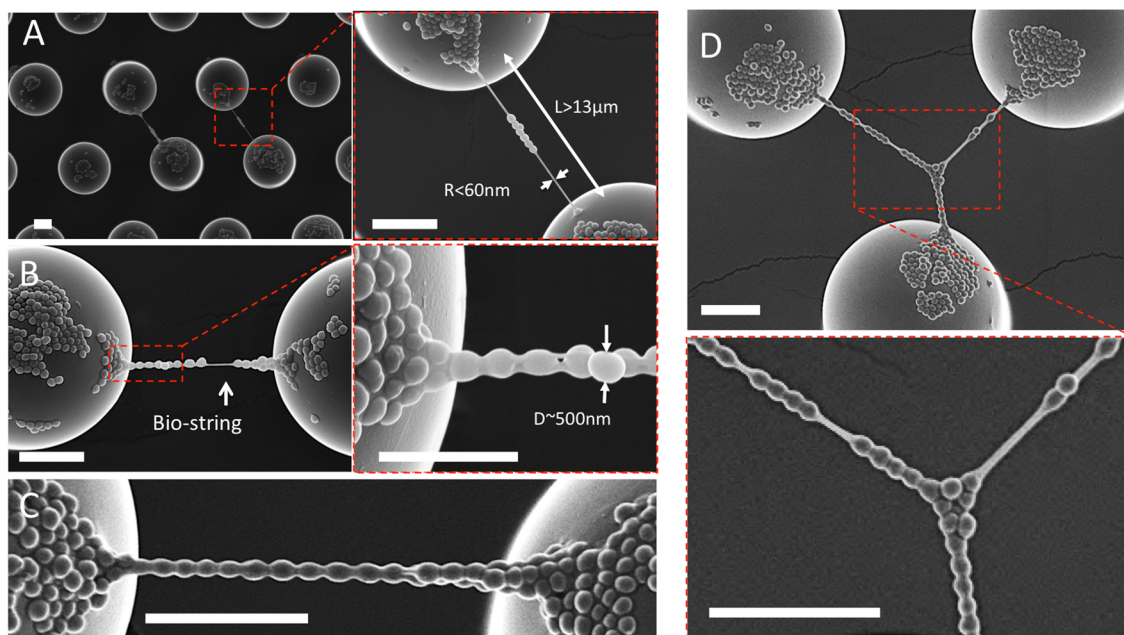


**Figure 3.** Formation of networks of *S. aureus* cells between neighboring micropillars. (A) Low (left) and high (right) magnification SEM images of strings with nanometer-scale radii ( $r < 60$  nm) and micrometer-scale lengths ( $L > 13$   $\mu\text{m}$ ) connecting two bacterial colonies on top of PDMS micropillars. (B) *S. aureus* cells with  $\sim 500$  nm diameters embedded inside biostrings and suspended between two adjacent micropillars. (C) A string of *S. aureus* cells connecting two adjacent bacterial colonies. (D) Biostrings of *S. aureus* cells connecting three adjacent micropillars and forming a network of *S. aureus* cells. All scale bars represent 5  $\mu\text{m}$ .

On the other hand, the liquid can partially sit on air pockets trapped between the solid surface asperities leading to superhydrophobic condition.<sup>40</sup> This regime is known as Cassie–Baxter regime and is formulated as

$$\cos \theta^C = -1 + f(1 + \cos \theta)$$

$\theta$  is the Young's contact angle on a flat surface,  $\theta^C$  and  $\theta^W$  are the Cassie–Baxter and Wenzel contact angles, respectively, while  $r$  and  $f$  represent roughness factor and the area fraction of the liquid–solid interface. Equating these two formulas defines a threshold contact angle  $\theta^*$ , which indicates the transition between Cassie–Baxter and Wenzel states.

$$\cos \theta^* = (f - 1)/(r - f)$$

According to this equation, the presence of air pockets at the interface and accordingly Cassie regime is favorable only if  $\theta \geq \theta^*$ .<sup>41</sup> To obtain more insight about our system, theoretical Cassie–Baxter and Wenzel state contact angles were calculated similar to the method described in a previous work.<sup>42</sup> Roughness factor,  $r$ , and area fraction of the liquid/solid interface,  $f$ , were determined using the following equations for a hexagonal array of cylindrical micropillars:

$$r = \frac{4\pi dh}{2\sqrt{3}i^2} + 1$$

$$f = \frac{2\pi d^2}{4\sqrt{3}i^2}$$

where  $h$ ,  $d$ , and  $i$  denote the pillars' height, diameter, and center-to-center spacing, respectively. We measured contact angle values for saline and nutrient broth solutions on PDMS platforms with various surface coverage percentages of micropillars and calculated the theoretical values for  $r$ ,  $f$ ,  $\theta$ , and  $\theta^*$  as tabulated in Table 1. The contact angle for the saline

solution on the control flat sample is consistently greater than  $\theta^*$  for all micropillar samples. Thus, Cassie–Baxter regime may be more favorable suggesting the presence of air pockets between micropillar arrays and the liquid surface. Accordingly, when the platform was submerged into a saline solution, the liquid contact line was pinned at the interface between the micropillars and flat PDMS surface (Figure 1E). On the other hand, except the micropillar sample with the maximum surface coverage of 33%,  $\theta^*$  is higher than the contact angle of the nutrient broth solution on the control flat sample for all other micropillar surfaces, indicating that the presence of air pockets underneath the droplet is less favorable for the nutrient broth solution. In fact, although closer to Cassie–Baxter regime, the drop of nutrient broth on the micropillars may be in the metastable state, thus, more inclined to transit between Wenzel and Cassie regimes.<sup>41</sup> Indeed, we observed the transition to Wenzel state when our sample was immersed in the nutrient broth solution where the solution gradually started penetrating into the surface incisions after 1 h (Figure 1E).

**Adhesion Characteristics of *S. aureus* Bacterial Cells on PDMS Micropillars.** *S. aureus* cells in a saline solution were plated on the PDMS platform as shown in Figure 2A and incubated for 1, 4, or 24 h. As predicted by wetting studies, adhered bacterial cells only remained on the top surface of micropillars when the sample was aspirated after a 1–4 h incubation time (Figure 2B), as the saline solution likely did not penetrate between micropillars during this time frame. Both side-view and top-view SEM images, and top view optical images indicated the adhesion of bacteria to the pillar tops as well as the flat PDMS surfaces at 1 and 4 h incubation times, with a higher density of adhered cells for longer incubation times of 4 h as expected (Figure 2B). However, after 24 h of incubation, bacterial cells fully covered the PDMS platform indicating that the solution penetrated into the surface asperities after 24 h and created a fully wetted condition. The

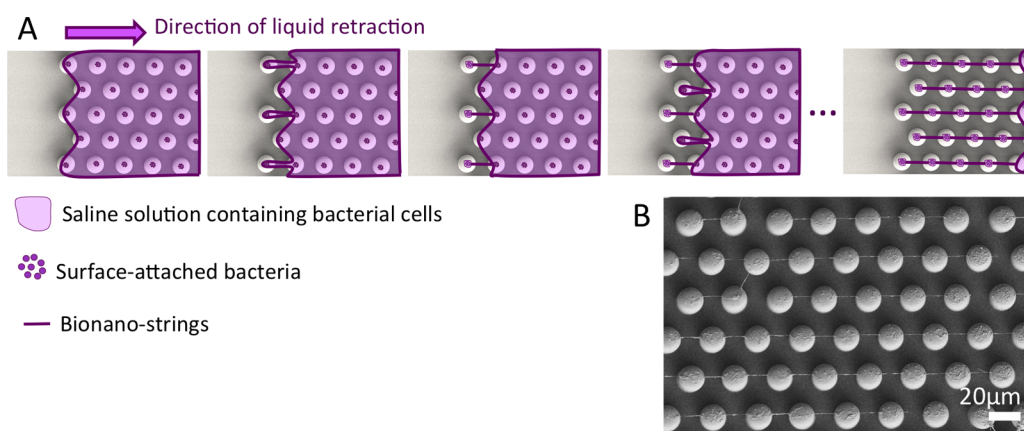


**Figure 4.** Schematic representation of mechanisms of biostring formation. (A) For short incubation times, the solution containing *S. aureus* bacterial cells sits on top of the hydrophobic PDMS micropillars and does not penetrate between micropillars. A thin biofilm or pellicle then forms on top of these micropillars (at the bottom of the *S. aureus* solution), while several bacterial cells actively adhere to the top surface of these micropillars. During the dewetting process, this biofilm collapses into thin biostrings, which form between bacterial colonies adhered on adjacent micropillars. These biostrings align in the direction of liquid retention in that location. (B) Locally aligned biostrings of *S. aureus* cells on top of PDMS micropillars.

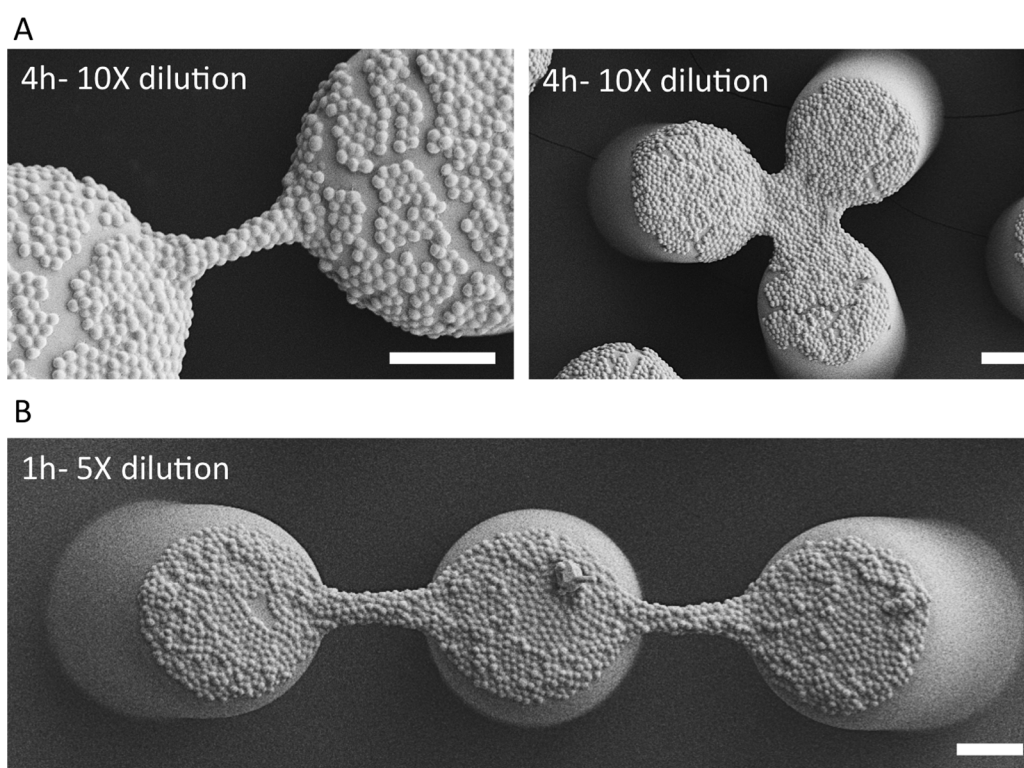


**Figure 5.** Control of biostring sizes by increasing bacteria incubation times or increasing cell densities. (A) SEM images of bacterial cells attached to and suspended between PDMS micropillars with a 1× cell density and 4 h incubation times. (B) SEM image of cells attached to and suspended between PDMS micropillars for 5× cell density and 1 h incubation times. All scale bars represent 5  $\mu\text{m}$ .

cracking of the layer of bacterial cells (for 4 and 24 h incubation times) and clustering of micropillars (for 24 h incubation time) as seen in Figure 2B is a result of the drying process for SEM preparation. Using the remarkable saline-solution repelling properties of these PDMS micropillars, through a single-step aspiration technique, we were able to pattern small isolated microcolonies of bacterial cells on top of PDMS micropillars. By changing bacteria incubation times, the size of microcolonies of *S. aureus* cells can be controlled. Furthermore, using PDMS micropillar arrays of different surface coverage areas (i.e., different distance between micropillars) colonies with

varying separation distances can be patterned (Table 1, Figure S1).

#### Fabrication of Biostrings of *S. aureus* Cells between PDMS Micropillars through Physiochemical Processes.

Detailed SEM inspections of the PDMS micropillar platforms that were aspirated after 1 h of bacteria incubation revealed several nanometer-scale string-like structures suspended between two (Figure 3A–C) or three (Figure 3D) bacteria microcolonies on adjacent micropillars. These high aspect ratio “biostrings” consisted of one or several round  $\sim 500$  nm diameter *S. aureus* cells aligned side by side between

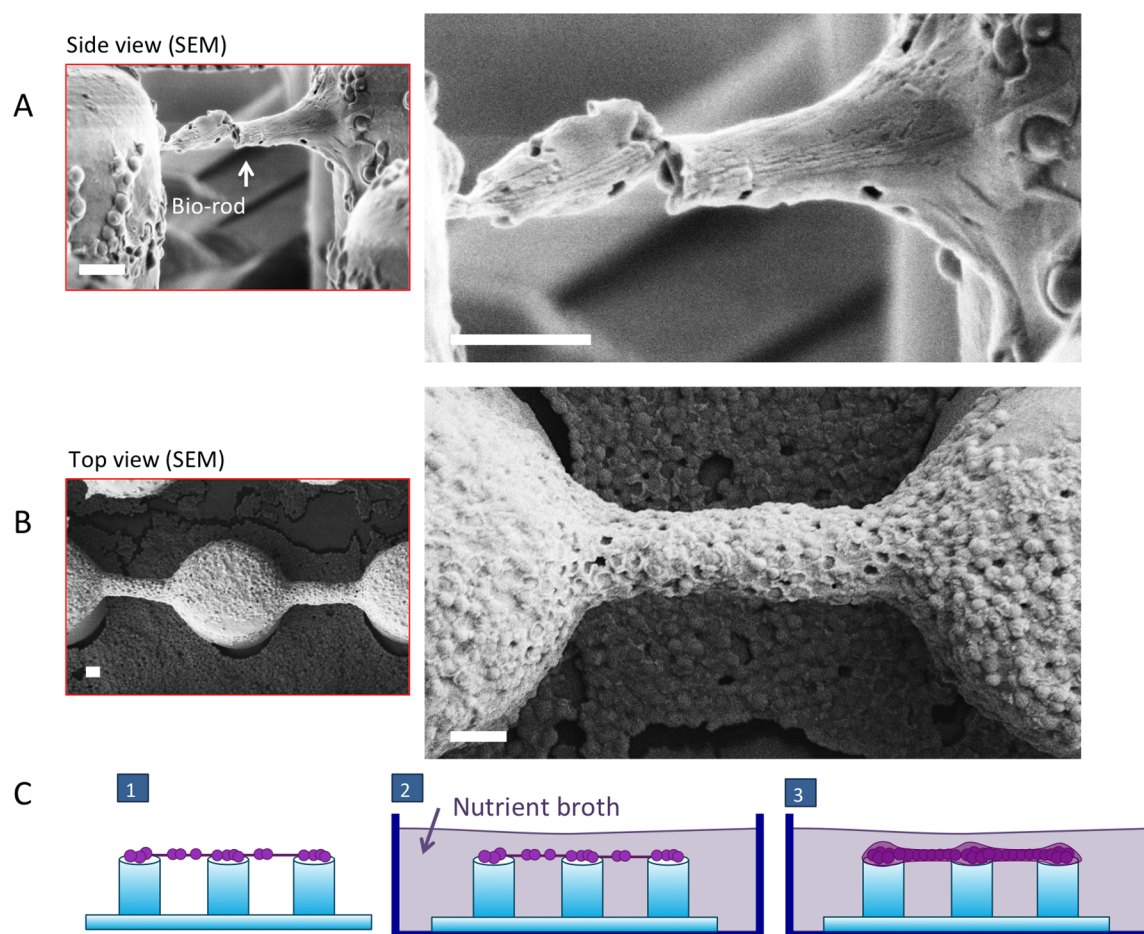


**Figure 6.** Growth of micrometer-thick rod shaped bacterial colonies (biorods) from biostrings. (A) Top and (B) side view SEM images of biorods formed between two adjacent micropillars. (C) Schematic representation of biorod formation: (1) biostrings were fabricated by dewetting PDMS micropillar arrays after 1 h of *S. aureus* incubation; (2) platforms were immediately placed into a solution of nutrient broth for 24 h; (3) strings of cells connecting adjacent micropillars grew into rod shaped biofilms or “biorods”.

micropillars as shown in Figure 3. Note that we name these microcolonies “biostrings” instead of “biofilms” since the bacterial cells are embedded into strings rather than films. In order to assess whether the dehydration step for SEM analysis was resulting in the formation of these biostrings, we imaged our PDMS platforms using optical microscopy directly after aspirating the bacteria solution and before sample dehydration. We observed similar biostrings forming between microposts (Figure S1). Furthermore, such biostrings were observed on PDMS micropillar arrays of various surface coverages (27–33%); however a higher number of biostrings were obtainable on platforms with higher surface area coverage of micropillars (Figure S1).

Next, we examined whether the formation of biostrings of *S. aureus* was due to active adhesion and activity of *S. aureus* cells or purely a physicochemical phenomenon resulting in a mere deposition of cells during the dewetting process by mechanisms similar to some previous studies. These studies used wetting/dewetting characteristics of PDMS micropillars to deposit and suspend highly ordered arrays of DNA nanowires on top of micropillars.<sup>33–38</sup> To test this, we fixed *S. aureus* cells in solution and plated these dead cells onto PDMS micropillar platforms and aspirated the samples after 1 h incubation. Careful inspections showed no *S. aureus* cell deposition on PDMS micropillars and no network formation (Figure S2). We concluded that in addition to the wetting properties of

hydrophobic PDMS micropillars, the formation of networks depended on biological processes, namely, the active adhesion of bacteria on pillar tops and the formation of thin biofilms at the bottom surface of the solution, which was not achievable with inactive bacteria.

The proposed mechanism of biostring formation is depicted in Figure 4A. During the 1 h incubation of bacterial solution on PDMS micropillars, *S. aureus* cells adhere to the solid surfaces that are available to them, specifically the flat PDMS surface and the top surfaces of micropillars. A thin biofilm or pellicle then begins to form at the bottom of the *S. aureus*-containing saline solution (on top of micropillars). During the sample aspiration and washing process, all *S. aureus* cells that are not strongly attached to any solid surfaces are removed. As the bacteria solution is extracted from the PDMS platform, the thin biofilm collapses into nanostrings suspended between micropillars. Furthermore, during this dewetting process, *S. aureus* cells in the solution that may be sitting on top of air gaps between micropillars get captured in the collapsing biofilm and form a string of bacterial cells embedded within a collapsed biofilm, which we refer to as “biostrings” (Figure 3, Figure 4). The direction of biostring formation depends on the local direction of liquid retraction from the micropillars (Figure 4B). Indeed Lin et al. modeled the dewetting mechanisms of hexagonally arranged PDMS micropillar arrays and showed that the alignment of DNA nanowires on top of micropillars is

highly dependent on the direction of dewetting as well as the arrangement of the micropillars.

Additionally, increasing either the incubation time (Figure 5A) or the initial concentration of *S. aureus* cells in the saline solution before plating cells (Figure 5B), allowed the control of the number of *S. aureus* cells attached to the top surfaces of micropillars and embedded within biostrings suspended between micropillars as shown in Figure 5. Using this simple technique, we were able to pattern bacterial colonies of varying sizes at the liquid–solid (bacteria solution and PDMS micropillars) and liquid–air (bacteria solution and air-pockets) interfaces. As we show in the next section, these microcolonies can later grow in a controlled manner, into biofilm-like structures with distinct architectures.

**Biorods of *S. aureus* Cells formed between PDMS Micropillars.** We next asked whether the *S. aureus* cells that were exposed to the dewetting process for biostring fabrication were able to grow into larger colonies. To test this, directly after aspirating the samples, we submerged the platform in a nutrient broth environment that induces *S. aureus* cell growth and incubated the sample for 24 h. As opposed to the conventional heterogeneous growth of bacterial colonies (biofilms) on flat surfaces,<sup>43</sup> the bacterial cells embedded in the biostrings suspended between micropillars developed into organized micrometer-thick rod shaped structures, which we refer to as “biorods” as shown in Figure 6A,B. As previously mentioned, air pockets are less likely to form between micropillars in the nutrient broth solution compared with the saline solution (Figure 1E, Figure S3). Therefore, the nutrient broth solution reaches a Wenzel state and creates a fully wetted condition on the submerged PDMS platform consisting of biostrings, allowing their access to nutrients and subsequently their growth into biorods after 24 h as shown in Figure 6C. In order to ensure that the biorods were in fact growing from the biostrings and not arbitrarily, in this step, we only fabricated biostrings in the center of the micropillar platform. Accordingly, we incubated a drop of bacteria-containing saline solution in the center of the platform, instead of submerging the entire PDMS platform in bacteria solution. After aspirating the drop, biostrings only formed in the areas covered by the drop. Consequently, after submersion into a nutrient broth solution for 24 h, biorods were only observed in the central regions of the PDMS platforms.

The communications between cells in a bacterial colony depend on several factors including their density and spatial distribution, as well as their surrounding environment; however, the various factors affecting bacterial communication are difficult to differentiate. Using our method, the activities of microcolonies attached to pillar tops can be compared with cells embedded in a thin matrix (the biostrings) and characterized side-by-side (Figure 7A). For example, future live-cell studies on bacterial cells on top of PDMS micropillars, compared with their neighboring biostrings can reveal phenotypical differences between solid-surface-associated and matrix-associated cell colonies in a highly controlled environment (Figure 7A). Generally, surface-anchored *S. aureus* cells grow into porous nonhomogeneous shaped biofilms on flat surfaces (Figure 7B). The suspended *S. aureus* cells on our PDMS platform showed a more homogeneous radial growth from nanostring structures into micrometer-thick rod-shaped structures. All previous studies of bacteria patterning have focused on patterning cells on solid surfaces with the goal of characterizing biofilm formation at the solid–liquid inter-

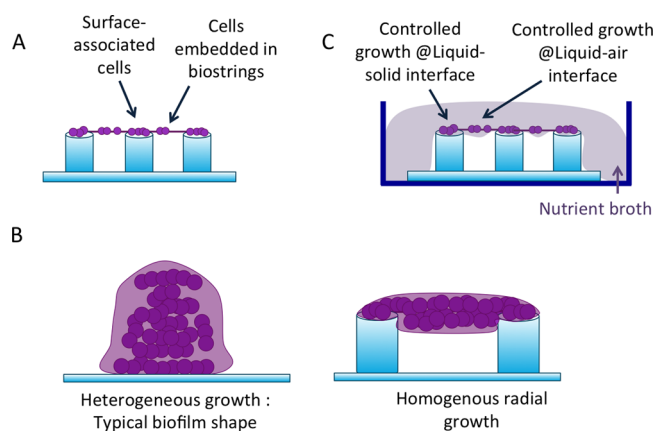


**Figure 7.** Potential applications for the developed cell patterning method. (A) Characterization of intercellular communications and colony growth in surface associated bacteria vs bacterial cells embedded within a thin biostring and suspended between micropillars. (B) Controlling a homogeneous radial growth of *S. aureus* colonies as opposed to typical heterogeneous biofilms on solid surfaces. (C) Control and comparison of colony growth at the liquid–solid or liquid–air interface by taking advantage of the wetting properties of PDMS micropillars.

face,<sup>12,23,27–29</sup> while bacterial colonies can also grow at a liquid air interface. Using closely spaced micropillars with surface coverage of 33% or more (Table 1), the nutrient broth solution also enters the Cassie–Baxter regime meaning that air pockets will form between the PDMS micropillars and so biostrings can grow controllably at the liquid–air interface mimicking the environment of pellicle formation (Figure 7C). Using this method, the anaerobic vs aerobic *S. aureus* colony growth could be characterized.

Finally, as shown in computational models by Lin et al., controlling the direction and speed of liquid extraction can precisely control the dewetting patterns of PDMS micropillars<sup>36</sup> and hence efficiently generate large arrays of highly ordered and interconnected colonies of bacteria.

## CONCLUSIONS

Bacterial cells have extraordinary communication skills and the capacity to colonize and form social networks in which they develop distinct phenotypes that drastically increase their chances of survival. Understanding the mechanisms of colony formation is therefore of great practical and clinical significance and requires the design of tools that can precisely control the initial organization and subsequent growth of bacterial colonies.

In this study, we developed a low-cost and simple method that utilizes surface dewetting properties of PDMS micropillars together with bacterial physiology to pattern nano- and micrometer scale colonies of methicillin-resistant *S. aureus*. Furthermore, we controlled colony growth architecture and showed that when provided with a nutrient rich environment, the patterned cells can grow into rod-shaped structures.

We believe our developed method can serve as a platform for studying the aerobic and anaerobic growth of bacterial colonies with a significant impact on understanding cell–cell communications such as quorum sensing, horizontal gene transfer, and metabolic cross-feeding specially during initial stages of colony formation. Our future studies will be directed at elucidating the effect of spatial control of *S. aureus* colonies on cell–cell communications and extracting the properties of the generated

birods and comparing them with conventional biofilms grown on flat solid surfaces.

## METHODS

**Fabrication of Micropillars.** Hexagonally arranged arrays of micropillars were replicated from a negative silicon master mold through casting of liquid poly(dimethylsiloxane) (Sylgard 184, Dow Corning) containing 10 wt % cross-linking agent and curing for 1 h at 120 °C. Diameter and the height of the micropillars were fixed at 15 and 22.5  $\mu\text{m}$ , respectively. Center-to-center spacing was varied between 25 and 32.5  $\mu\text{m}$  yielding 33% to 19% micropillar surface coverage (*f*). To avoid any defect to the pillars during the peeling, the surface of the master mold was treated with self-assembled monolayers (SAM) of heptadecafluoro-1,1,2,2-tetrahydrodecyltrichlorosilane (Gel-est Inc. MA, USA) using the methods described elsewhere.<sup>44</sup>

**Contact Angle Measurement.** Sessile drop technique was used for static contact angle measurements using a custom-made apparatus. Droplets of saline solution and nutrient broth with volumes of about 5  $\mu\text{L}$  were dispensed on the samples at the rate of 100 mL/h. At least 10 images of the liquid droplets on the surfaces were analyzed to extract the contact angle at the three-phase contact line.

***S. aureus* Culture and Plating.** *S. aureus* (ATCC 6538) was purchased from Cedarlane Laboratories (Burlington, ON, Canada). *S. aureus* was inoculated on Trypticase Soy Agar (TSA) plates and incubated at 37 °C for 24 h. Bacterial cells were harvested using alginate swabs and suspended in 5 mL of sterile saline (2.55%) with nutrient broth (~0.006%) in a 15 mL centrifuge tube. A 2.55% saline solution was prepared and sterilized by using Nalgene filters. In order to preserve *S. aureus* cells during experiments, 0.006% of nutrient broth was added to the saline solution. *S. aureus* cells were then transferred to the saline solution by adding 5 mL of saline to the TSA plate. *S. aureus* cells were washed with saline solution seven times by centrifugation at 4000 rpm for 10 min. The stock solution of *S. aureus* cells was diluted 10-fold or 5-fold in saline for low- or high-density cell patterning, respectively.

For each experiment, the PDMS platforms were placed inside a Petri dish and 4.5 mL of the diluted *S. aureus* solution was added until the solution covered the entire platform (Figure 2A). The platforms were then incubated at 37 °C for 1, 4, or 24 h. Subsequently, the samples were aspirated to remove bacterial solution and either imaged immediately using optical microscopy or prepared for SEM analysis. Alternatively for biorod fabrication, aspirated samples were placed into a Petri dish containing BD BBL Prepared Nutrient Broth and incubated at 37 °C for 24 h before fixation and imaging. As a control for this experiment, an identical sample was fixed and dried directly after aspiration and observed under the SEM.

**SEM Preparation and Imaging.** *S. aureus* cells were fixed using 2.5% glutaraldehyde for 2 h and air-dried in a fume hood for 12 h. The PDMS samples were then coated with a 10 nm layer of gold and inspected using a field emission scanning electron microscope (Zeiss LEO 1550).

## ASSOCIATED CONTENT

### Supporting Information

The Supporting Information is available free of charge on the ACS Publications website at DOI: 10.1021/acsnano.6b06985.

Optical images of PDMS platforms of varying micropillar surface coverage, SEM image of platforms where bacteria were fixed in solution before plating on PDMS microposts, and adhesion patterns of bacteria plated onto PDMS microposts after 1 or 4 h incubation (PDF)

## AUTHOR INFORMATION

### Corresponding Author

\*E-mail: mofrad@berkeley.edu.

## ORCID

Frank X. Gu: 0000-0001-8749-9075

## Notes

The authors declare no competing financial interest.

## REFERENCES

- (1) Hutchison, J. B.; Rodesney, C. A.; Kaushik, K. S.; Le, H. H.; Hurwitz, D. A.; Irie, Y.; Gordon, V. D. Single-Cell Control of Initial Spatial Structure in Biofilm Development Using Laser Trapping. *Langmuir* **2014**, *30*, 4522.
- (2) Díaz, C.; Schilardi, P. L.; Dos Santos Claro, P. C.; Salvezza, R. C.; Fernández Lorenzo De Mele, M. A. Submicron Trenches Reduce the *Pseudomonas Fluorescens* Colonization Rate on Solid Surfaces. *ACS Appl. Mater. Interfaces* **2009**, *1* (1), 136–143.
- (3) Kastrup, C. J.; Boedicker, J. Q.; Pomerantsev, A. P.; Moayeri, M.; Bian, Y.; Pompano, R. R.; Kline, T. R.; Sylvestre, P.; Shen, F.; Leppla, S. H.; Tang, W.-J.; Ismagilov, R. F. Spatial Localization of Bacteria Controls Coagulation of Human Blood by “Quorum Acting”. *Nat. Chem. Biol.* **2008**, *4* (12), 742–750.
- (4) Shen, F.; Pompano, R. R.; Kastrup, C. J.; Ismagilov, R. F. Confinement Regulates Complex Biochemical Networks: Initiation of Blood Clotting By “Diffusion Acting”. *Biophys. J.* **2009**, *97* (8), 2137–2145.
- (5) Boedicker, J. Q.; Vincent, M. E.; Ismagilov, R. F. Microfluidic Confinement of Single Cells of Bacteria in Small Volumes Initiates High-Density Behavior of Quorum Sensing and Growth and Reveals Its Variability. *Angew. Chem., Int. Ed.* **2009**, *48* (32), 5908–5911.
- (6) Hansen, R. H.; Timm, A. C.; Timm, C. M.; Bible, A. N.; Morrell-Falvey, J. L.; Pelletier, D. A.; Simpson, M. L.; Doktycz, M. J.; Retterer, S. T. Stochastic Assembly of Bacteria in Microwell Arrays Reveals the Importance of Confinement in Community Development. *PLoS One* **2016**, *11* (5), e0155080.
- (7) Pande, S.; Shitut, S.; Freund, L.; Westermann, M.; Bertels, F.; Colesie, C.; Bischofs, I. B.; Kost, C. Metabolic Cross-Feeding via Intercellular Nanotubes among Bacteria. *Nat. Commun.* **2015**, *6*, 6238.
- (8) Bassler, B. L.; Losick, R. Bacterially Speaking. *Cell* **2006**, *125* (2), 237–246.
- (9) Jahed, Z.; Lin, P.; Seo, B. B.; Verma, M. S.; Gu, F. X.; Tsui, T. Y.; Mofrad, M. R. K. Responses of Staphylococcus Aureus Bacterial Cells to Nanocrystalline Nickel Nanostructures. *Biomaterials* **2014**, *35* (14), 4249–4254.
- (10) Wu, Y.; Zitelli, J. P.; TenHuisen, K. S.; Yu, X.; Libera, M. R. Differential Response of Staphylococci and Osteoblasts to Varying Titanium Surface Roughness. *Biomaterials* **2011**, *32* (4), 951–960.
- (11) Truong, V. K.; Lapovok, R.; Estrin, Y. S.; Rundell, S.; Wang, J. Y.; Fluke, C. J.; Crawford, R. J.; Ivanova, E. P. The Influence of Nano-Scale Surface Roughness on Bacterial Adhesion to Ultrafine-Grained Titanium. *Biomaterials* **2010**, *31* (13), 3674–3683.
- (12) Hochbaum, A. I.; Aizenberg, J. Bacteria Pattern Spontaneously on Periodic Nanostructure Arrays. *Nano Lett.* **2010**, *10* (9), 3717–3721.
- (13) Madsen, J. S.; Burmølle, M.; Hansen, L. H.; Sørensen, S. J. The Interconnection between Biofilm Formation and Horizontal Gene Transfer. *FEMS Immunol. Med. Microbiol.* **2012**, *65* (2), 183–195.
- (14) Remis, J. P.; Wei, D.; Gorur, A.; Zemla, M.; Haraga, J.; Allen, S.; Witkowska, H. E.; Costerton, J. W.; Berleman, J. E.; Auer, M. Bacterial Social Networks: Structure and Composition of Myxococcus Xanthus Outer Membrane Vesicle Chains. *Environ. Microbiol.* **2014**, *16* (2), 598–610.
- (15) Nudleman, E.; Wall, D.; Kaiser, D. Cell-to-Cell Transfer of Bacterial Outer Membrane Lipoproteins. *Science* **2005**, *309* (5731), 125–127.
- (16) Chiura, H. X.; Kogure, K.; Hagemann, S.; Ellinger, A.; Velimirov, B. Evidence for Particle-Induced Horizontal Gene Transfer and Serial Transduction between Bacteria. *FEMS Microbiol. Ecol.* **2011**, *76* (3), 576–591.
- (17) Yaron, S.; Kolling, G. L.; Simon, L.; Matthews, K. R. Vesicle-Mediated Transfer of Virulence Genes from Escherichia Coli

- O157:H7 to Other Enteric Bacteria. *Appl. Environ. Microbiol.* **2000**, *66* (10), 4414–4420.
- (18) Miller, M. B.; Bassler, B. L. QUORUM SENSING IN BACTERIA. *Annu. Rev. Microbiol.* **2001**, *55*, 165–189.
- (19) Chiu, H.-C.; Lee, S.-L.; Kapuriya, N.; Wang, D.; Chen, Y.-R.; Yu, S.-L.; Kulp, S. K.; Teng, L.-J.; Chen, C.-S. Development of Novel Antibacterial Agents against Methicillin-Resistant *Staphylococcus Aureus*. *Bioorg. Med. Chem.* **2012**, *20* (15), 4653–4660.
- (20) Holden, M. T. G.; Feil, E. J.; Lindsay, J. a; Peacock, S. J.; Day, N. P. J.; Enright, M. C.; Foster, T. J.; Moore, C. E.; Hurst, L.; Atkin, R.; Barron, A.; Bason, N.; Bentley, S. D.; Chillingworth, C.; Chillingworth, T.; Churcher, C.; Clark, L.; Corton, C.; Cronin, A.; Doggett, J.; Dowd, L.; Feltwell, T.; Hance, Z.; Harris, B.; Hauser, H.; Holroyd, S.; Jagels, K.; James, K. D.; Lennard, N.; Line, A.; Mayes, R.; Moule, S.; Mungall, K.; Ormond, D.; Quail, M. a; Rabinowitsch, E.; Rutherford, K.; Sanders, M.; Sharp, S.; Simmonds, M.; Stevens, K.; Whitehead, S.; Barrell, B. G.; Spratt, B. G.; Parkhill, J. Complete Genomes of Two Clinical *Staphylococcus Aureus* Strains: Evidence for the Rapid Evolution of Virulence and Drug Resistance. *Proc. Natl. Acad. Sci. U. S. A.* **2004**, *101* (26), 9786–9791.
- (21) Cosgrove, S.; Sakoulas, G.; Perencevich, E.; Schwaber, M.; Karchmer, A.; Carmeli, Y. Comparison of Mortality Associated with Methicillin Resistant and Methicillin Susceptible *Staphylococcus Aureus* Bacteremia: A Meta-Analysis. *Clin. Infect. Dis.* **2003**, *36* (1), 53–59.
- (22) Foster, T. J.; Geoghegan, J. A.; Ganesh, V. K.; Höök, M. Adhesion, Invasion and Evasion: The Many Functions of the Surface Proteins of *Staphylococcus aureus*. *Nat. Rev. Microbiol.* **2014**, *12*, 49–62.
- (23) Kim, J.; Shin, Y. H.; Yun, S. H.; Choi, D. S.; Nam, J. H.; Kim, S. R.; Moon, S. K.; Chung, B. H.; Lee, J. H.; Kim, J. H.; Kim, K. Y.; Kim, K. M.; Lim, J. H. DPN104-Direct-Write Patterning of Bacterial Cells by Dip-Pen Nanolithography. *J. Am. Chem. Soc.* **2012**, *134* (40), 16500–16503.
- (24) Weibel, D. B.; Lee, A.; Mayer, M.; Brady, S. F.; Bruzewicz, D.; Diluzio, W.; Clardy, J.; Whitesides, G. M.; Yang, J. Bacterial Printing Press That Regenerates Its Ink: Contact Printing Bacteria Using Hydrogel Stamps. *Langmuir* **2005**, *21*, 6436 see Supporting Information.
- (25) Xu, L.; Robert, L.; Ouyang, Q.; Taddei, F.; Chen, Y.; Lindner, A. B.; Baigl, D. Microcontact Printing of Living Bacteria Arrays with Cellular Resolution. *Nano Lett.* **2007**, *7* (7), 2068–2072.
- (26) Weibel, D. B.; Diluzio, W. R.; Whitesides, G. M. Micro-fabrication Meets Microbiology. *Nat. Rev. Microbiol.* **2007**, *5* (3), 209–218.
- (27) Suo, Z.; Avci, R.; Yang, X.; Pascual, D. W. Efficient Immobilization and Patterning of Live Bacterial Cells. *Langmuir* **2008**, *24* (8), 4161–4167.
- (28) Palacios-Cuesta, M.; Cortajarena, A. L.; Garcia, O.; Rodriguez-Hernandez, J. Patterning of Individual *Staphylococcus Aureus* Bacteria onto Photogenerated Polymeric Surface Structures. *Polym. Chem.* **2015**, *6*, 2677–2684.
- (29) Epstein, a K.; Hochbaum, a I.; Kim, P.; Aizenberg, J. Control of Bacterial Biofilm Growth on Surfaces by Nanostructural Mechanics and Geometry. *Nanotechnology* **2011**, *22* (49), 494007.
- (30) Nait Chabane, Y.; Marti, S.; Rihouey, C.; Alexandre, S.; Hardouin, J.; Lesouhaitier, O.; Vila, J.; Kaplan, J. B.; Jouenne, T.; Dé, E. Characterisation of Pellicles Formed by *Acinetobacter Baumannii* at the Air-Liquid Interface. *PLoS One* **2014**, *9* (10), e111660.
- (31) Zara, S.; Bakalinsky, A. T.; Zara, G.; Demontis, M. A.; Budroni, M.; Pirino, G. FLO11 -Based Model for Air-Liquid Interfacial Biofilm Formation by *Saccharomyces Cerevisiae* FLO11 -Based Model for Air-Liquid Interfacial Biofilm Formation by *Saccharomyces Cerevisiae*. *Appl. Environ. Microbiol.* **2005**, *71* (6), 2934–2939.
- (32) Mielich-Süss, B.; Lopez, D. Molecular Mechanisms Involved in *Bacillus Subtilis* Biofilm Formation. *Environ. Microbiol.* **2015**, *17* (3), 555–565.
- (33) Glazer, P. J.; Bergen, L.; Jennings, L.; Houtepen, A. J.; Mendes, E.; Boukany, P. E. Generating Aligned Micellar Nanowire Arrays by Dewetting of Micropatterned Surfaces. *Small* **2014**, *10* (9), 1729–1734.
- (34) Guan, J.; Yu, B.; Lee, L. J. Forming Highly Ordered Arrays of Functionalized Polymer Nanowires by Dewetting on Micropillars. *Adv. Mater.* **2007**, *19* (9), 1212–1217.
- (35) Miele, E.; Accardo, A.; Falqui, A.; Marini, M.; Giugni, A.; Leoncini, M.; De Angelis, F.; Krahne, R.; Di Fabrizio, E. Di. Writing and Functionalisation of Suspended DNA Nanowires on Superhydrophobic Pillar Arrays. *Small* **2015**, *11* (1), 134–140.
- (36) Lin, C. H.; Guan, J.; Chau, S. W.; Chen, S. C.; Lee, L. J. Patterning Nanowire and Micro-/nanoparticle Array on Micropillar-Structured Surface: Experiment and Modeling. *Biomicrofluidics* **2010**, *4* (3), 034103.
- (37) Charlot, B.; Bardin, F.; Sanchez, N.; Roux, P.; Teixeira, S.; Schwob, E. Elongated Unique DNA Strand Deposition on Microstructured Substrate by Receding Meniscus Assembly and Capillary Force. *Biomicrofluidics* **2014**, *8* (1), 014103.
- (38) Guan, J.; Lee, L. J. Generating Highly Ordered DNA Nanostrand Arrays. *Proc. Natl. Acad. Sci. U. S. A.* **2005**, *102* (S1), 18321–18325.
- (39) Wenzel, R. N. Resistance of Solid Surfaces to Wetting by Water. *Ind. Eng. Chem.* **1936**, *28*, 988–994.
- (40) Cassie, B. D.; Baxter, S. Wettability of Porous Surfaces. *Trans. Faraday Soc.* **1944**, *40* (5), 546–551.
- (41) Lafuma, A.; Quéré, D. Superhydrophobic States. *Nat. Mater.* **2003**, *2* (7), 457–460.
- (42) Shahsavan, H.; Arunbabu, D.; Zhao, B. Biomimetic Modification of Polymeric Surfaces: A Promising Pathway for Tuning of Wetting and Adhesion. *Macromol. Mater. Eng.* **2012**, *297* (8), 743–760.
- (43) Garrett, T. R.; Bhakoo, M.; Zhang, Z. Bacterial Adhesion and Biofilms on Surfaces. *Prog. Nat. Sci.* **2008**, *18* (9), 1049–1056.
- (44) Shahsavan, H.; Zhao, B. Conformal Adhesion Enhancement on Biomimetic Microstructured Surfaces. *Langmuir* **2011**, *27*, 7732–7742.